PAPER

CrossMark
click for updates

Solar synthesized tin oxide nanoparticles dispersed on graphene wrapped carbon nanotubes as a Li ion battery anode material with improved stability†

Madhumita Sahoo and S. Ramaprabhu*

Employing high theoretical capacity SnO_2 as an anode material for Li ion batteries (LIBs) is still a challenge because of its huge volume change upon lithiation/de-lithiation, leading to instability and a low cycle life of the cell. Herein we report graphene wrapped carbon nanotubes (gC), a one-dimensional monohybrid of multiwalled carbon nanotubes and graphene sheets, which support SnO_2 nanoparticles to act as a stable LIB anode. An eco-friendly, solar energy mediated reduction process, instead of hazardous wet chemical methods, was used to decorate SnO_2 over the gC support material. The wrinkled surface of gC, with a higher available surface area and favorable Li transfer channels, is explored as a functional preventive measure against the volume change of the metal oxide nanoparticles. This well-connected gC structure with high conductivity also accounts for the semiconducting nature of SnO_2, and exhibits less resistance with a highly stable performance, thereby presenting SnO_2/gC as a potential anode material for LIBs.

Introduction

The present ecological concerns of civilization demand sustainable, pollution-free, clean and cost-effective renewable energy technologies. Solar, tidal and wind energies are natural energies that need storage systems associated with them for uninterrupted usage. The Li ion battery (LIB) has emerged as an important rechargeable electrochemical conversion and storage device because of its many advantages, such as high energy density, capacity, and cycle life, over the past two decades.[1] The commercially used graphite anode in LIBs limits the battery performance owing to its low specific capacity of 372 mA h g^{-1}.[2] The high abundance of SnO_2 in nature has projected itself as a low cost and favorable material for biosensors,[3] capacitors[4] and many more applications,[5] including as an anode material in LIBs.[6] The problem of the huge (~300%) volume change[7] of SnO_2 during lithiation/de-lithiation cycles, leading to unavoidable pulverization still demands further structural engineering for it to be to be an efficient and stable anode material. Even after much research over the last few decades, the volume variation of SnO_2 still leads to a poor life-cycle and rate performance. The capacity fading is also a result of pulverization of tin oxide, leading to mechanical disintegration and fresh surface exposures of the active material which results in the continuous formation of solid electrolyte interface (SEI) layer. 3 nm SnO_2 nanoparticles have been reported to show enhanced performance owing to less aggregation into clusters.[8] To prevent the active material loss over mechanical degradation, the design of hollow[9] and core–shell[10] metal oxide nanostructures, as well as the use of an accommodating and conducting support structure, has been implemented by the research community. 1D carbon nanotubes (CNT),[11] 2D graphene[12,13] and their hybrid[14,15] structures have been well investigated as supports for SnO_2 nanoparticles. 1D–2D composite structures of a MWNT-graphene support in a nano-3D aerogel form for SnO_2 support,[16] polypyrrole based carbon nanowire-graphene supported SnO_2,[17] a one-pot microwave synthesized SnO_2/G-CNT composite,[18] and a hydrazine reduced hybrid SnO_2/G-CNT[15] are a few examples of the many investigated anode materials. However a commercially available, stable and high performance tin oxide composite has not been reported until now, as the reported composites have flaws such as complicated synthesis processes, hazardous chemical usage, a demand for wet production processes or uniformity in the structure.[20–23]

The present report investigates protruded surface 1D monohybrid-graphene wrapped carbon nanotubes (gC) as the support for the tin oxide nanoparticles and the application of the composite as an anode material in a Li ion battery. The unique structural and morphological features of gC have already proved that it is a better anode material than commercial graphite.[19] A simple, inexpensive and environmentally benign solar reduction synthesis process has been used for the uniform dispersion of tin oxide nanoparticles over the graphene wrapped carbon nanotubes. The tin oxide nanoparticles, which

Alternative Energy and Nanotechnology Laboratory (AENL), Nano-Functional Materials and Technology Centre (NFMTC), Department of Physics, IIT Madras, Chennai-600036, India. E-mail: ramp@iitm.ac.in

enable better Li diffusion, and the conducting structure of gC facilitating electron transfer, are expected to raise the minimum stress in the lithiation/delithiation process because of the wrinkled surface and the porous nature of the support, giving sufficient void space for accommodation of the volume variation.

Experimental

Material synthesis

The decoration of tin oxide nanoparticles over gC was performed using a green solar reduction technique, and the material was employed as an anode in a Li ion battery. Pure graphene wrapped carbon nanotubes were synthesized using a modified catalyst assisted chemical vapor deposition (CCVD) technique (S.I.) as reported by us previously.[19,24] A tin chloride di-hydrate ($SnCl_2 \cdot 2H_2O$; ≥99.995%; Aldrich) precursor was mechanically mixed in a ratio of 1 : 3 with graphene wrapped carbon nanotubes. Solar energy was focused using a convex lens (90 mm diameter) to act as the energy source for the reduction.[26] The previously prepared mixture was uniformly spread on a glass Petri dish and exposed to the focused solar energy using the lens for a few minutes during peak hours of scorching heat on a clear summer day. The exposure was scanned throughout the spread sample in an identical method for uniformity. The temperature of the focused portion increased rapidly to 150–450 °C within a few seconds, resulting in decomposition of the precursor salt and the simultaneous deposition of tin nanoparticles over the support surface.[25,26] The release of gaseous by-products was clearly visible during the short time of the synthesis. Tin nanoparticles reacted with atmospheric oxygen and oxygen that was decomposing from the salt, resulting in tin oxide nanoparticles, owing to the chemical reactivity of tin at high temperatures. Finally, the black powder was collected and labeled as SnO_2/gC without any further modifications. For comparison, SnO_2 nanoparticles were also decorated over the surfaces of purified multiwalled carbon nanotubes[27] (MWNT) using a similar process. Without any further treatment, the SnO_2/MWNT and SnO_2/gC materials were tested as anode materials for LIBs.

Physical characterization

A PANalytical X'Pert Pro X-ray diffractometer, with nickel filtered Cu-K_α radiation as the X-ray source, was used to record the X-ray diffraction (XRD) measurements over a 2θ range of 5–90° with a step size of 0.016°. The loading of metal oxide on the gC and MWNT support was calculated using the results from a thermogravimetric analysis plot, which was recorded using an SDTQ600 (TA instruments) analyzer in a zero-air atmosphere from room temperature (30 °C) to 1000 °C. A LabRAM HP 800 UV Raman spectrometer was used to study the vibrational modes of the samples, with a 632 nm He–Ne laser used as the excitation source, over the range of 1000–2000 cm^{-1}. An X-ray photoelectron spectroscopy (XPS) study was performed to check the phases of the synthesized materials, using a SPECS instrument with Mg-K_α as the X-ray source and PHOIBOS

100MCD as the analyzer under ultrahigh vacuum (10^{-10} mbar). CasaXPS software with Shirley background correction was used to deconvolute the data. A field emission scanning electron microscope (FESEM, FEI QUANTA3D) and a transmission electron microscope (FEI Technai G^2 20 STWIN, 200 keV) were used to characterize the morphologies of the samples. Elemental mapping analysis measurements were carried out using a FEI Quanta FEG 200 instrument. For the XPS and SEM analysis, the powder sample was uniformly coated on one side of some adhesive carbon tape, while for the TEM analysis, samples were prepared by drop-casting a few drops of the ethanol-dispersed material over a 200-mesh gold coated copper grid.

Electrochemical characterization

The electrode slurry was prepared by mixing the active material (SnO_2/gC or SnO_2/MWNT) with a polyvinylidene fluoride (PVDF) binder and conductive graphite in a ratio of 75 : 15 : 10 in an N-methyl-2-pyrrolidinone solvent. A doctor blade technique was used to uniformly coat the slurry onto the copper foil which was then dried in a vacuum oven at 120 °C for 6 h. 12 mm diameter anode coins were cut from the dried active-material slurry mixture on the copper foil. CR 2032 type coin cells with lithium metal as the counter electrode, Celgard 2400 as the membrane separator, and LiPF$_6$ (1 M) dissolved in a mixture of ethylene carbonate (EC) and dimethyl carbonate (DMC) (EC/DMC, 1 : 1 v/v) as the electrolyte, were employed for testing. The cells were fabricated in a high pure argon (>99.999%) filled glove box (mBRAUN, Unilab) for the electrochemical measurements. A Solartron electrochemical workstation was used to study the galvanostatic charge–discharge measurements between 3 V and 0.01 V at room temperature for the assembled coin cells. An Autolab PGSTAT302 instrument with NOVA software was used to obtain the cyclic voltammograms (CVs) and impedance spectra for the employed materials. CV was recorded at a scan rate of 0.5 mV s^{-1}, while a sine wave with an amplitude of 5 mV over a frequency range from 100 kHz to 0.01 Hz was applied to record the electrochemical ac impedance spectra.

Result and discussion

Fig. 1 shows a schematic of the SnO_2/gC synthesis process and the Li interaction pathways on the composite material. Graphene wrapped carbon nanotubes with wrinkled surface and comparative less length than MWNT was synthesized using CCVD technique as discussed earlier.[19] 35 mg of tin precursor was mixed with 105 mg of gC and sprinkled over a Petri-dish. Solar energy was concentrated through the lens, and focused uniformly over the sprinkled precursor mixture. The focused solar energy raises the local temperature to ~450° within a few seconds, thus decomposing the metal salt. As a result, tin nanoparticles attach to the gC support structure with the release of gaseous by-products. The non-noble metal nanoparticles react with atmospheric oxygen in those conditions, thus forming the tin oxide decorated graphene wrapped carbon nanotube structure.
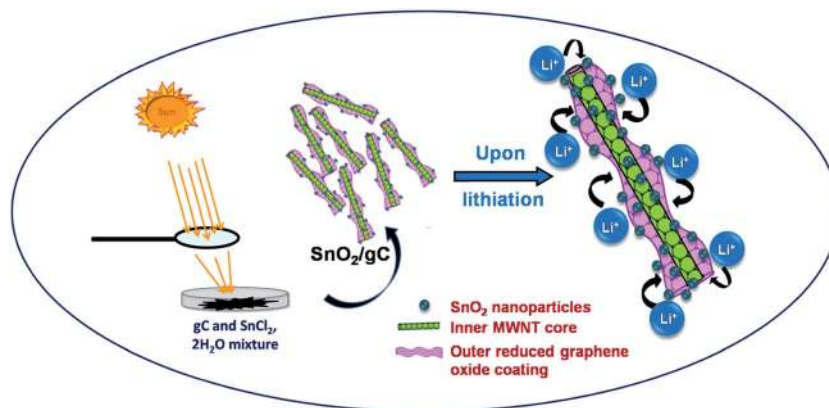
Fig. 1 Schematic representation of the synthesis of SnO_2/gC with the lithium interaction sites on gC.

X-ray diffraction patterns were recorded to confirm the formation of the support as well as the composite structure, and are shown in Fig. 2A for (a) MWNT, (b) gC, (c) SnO_2/MWNT and (d) SnO_2/gC. The characteristic C (002) peak at around 26° in Fig. 2A(a) for MWNT shows the long-range order of the synthesized multiwalled carbon nanotubes. Broadening in the base of C (002) peak in Fig. 2A(b) for gC emphasizes its disorder nature. There is no evidence of any remaining catalyst or graphite oxide in this diffraction pattern, thus highlighting the phase pure gC. Fig. 2A(c and d) shows the presence of a crystalline SnO_2 tetragonal phase, with (110), (101), (211) and (301) peaks at around 27°, 34°, 52° and 65.5°, respectively. C (002) of the support MWNT or gC structures is merged with the SnO_2 (110) phase. There was no sign of the presence of any other states of Sn in both the solar-synthesized SnO_2/MWNT and SnO_2/gC. The average crystallite sizes of the SnO_2 nanoparticles for SnO_2/MWNT and SnO_2/gC, calculated using Scherrer's formula,[28] are 3.1 nm and 2.8 nm, respectively. The thermal

stability and metal oxide loading of the composite powder samples were assessed using thermo-gravimetric analysis (TGA) which is presented in Fig. 2B. A ~26% loading of SnO_2, in contrast to the desired 30% loading, was observed over the gC support material using the solar reduction method (Fig. 2B(b)). The metal oxide loading was found to be ~27% for SnO_2/MWNT (Fig. 2B(a)). A Raman spectroscopy study was carried out on the materials to further confirm the formation of the desired phases of the materials. Fig. 3A shows the Raman spectra for (a) MWNT, (b) gC, (c) SnO_2/MWNT and (d) SnO_2/gC. All four samples showed characteristic D and G bands at around 1350 cm^{-1} and 1582 cm^{-1}, which represent the carbon backbone. The high I_D/I_G value (Table 1) for gC (Fig. 3A(b)) compared to MWNT (Fig. 3A(a)) is due to the surface defects in terms of wrinkles and protrusions. The decoration of tin oxide nanoparticles over the support increases the I_D/I_G ratio for SnO_2/MWNT (Fig. 3A(c)) while the ratio decreases for SnO_2/gC (Fig. 3A(d)). The peaks within the 400 to 700 cm^{-1} range for
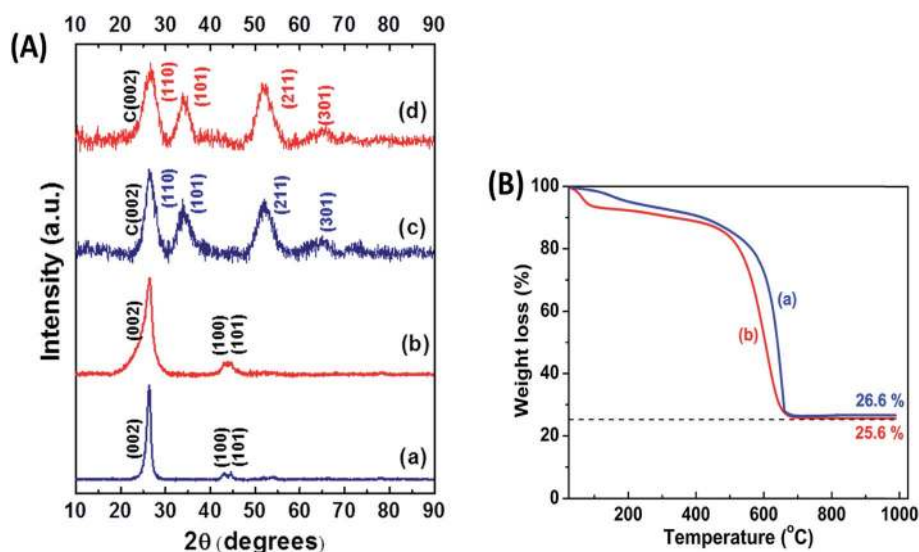

Fig. 2 (A) XRD patterns for (a) MWNT, (b) gC, (c) SnO_2/MWNT and (d) SnO_2/gC; (B) thermo-gravimetric analysis for (a) SnO_2/MWNT and (b) SnO_2/gC.
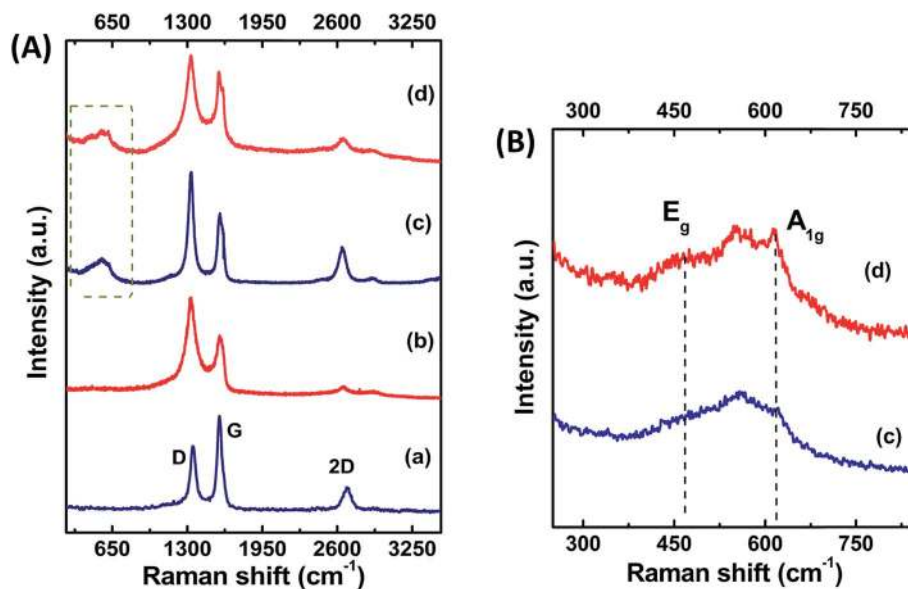
Fig. 3 (A) Raman spectra for (a) MWNT, (b) gC, (c) SnO_2/MWNT and (d) SnO_2/gC. The Raman modes of SnO_2 are shown in (B) for (c) SnO_2/MWNT and (d) SnO_2/gC.

Table 1 I_D/I_G ratios of the synthesized materials

Material	MWNT	gC	SnO_2/MWNT	SnO_2/gC
I_D/I_G value	0.36	1.48	1.62	1.23

Fig. 3A(c and d) show the Raman modes of the tin oxide nanoparticles which are absent in bare MWNT and gC. Fig. 3B presents a zoomed view of these Raman bands within the dotted area of Fig. 3A(c and d). The peaks at around 467 cm^{-1} and 622 cm^{-1} are attributed to the E_g and A_{1g} modes of the SnO_2 phase.[29] The broadened peak at around 565 cm^{-1} represents the surface defectiveness due to the smaller sizes of the dispersed tin oxide nanoparticles,[30] as already confirmed from the crystallite sizes. XPS measurements were performed to obtain information about the Sn phases obtained using the solar reduction technique. Fig. 4 shows (a) a survey spectrum, and deconvoluted (b) C 1s and (c) Sn 3d spectra for the synthesized SnO_2/gC material. The survey spectrum of Fig. 4a shows the desired presence of Sn, C and O, and a negligible amount of Cl residue from the reactant. The C 1s spectrum of the gC support exhibits four different contributions, arising from the C=C (284.5 eV), C–OH (286.4 eV), C=O (288.5 eV), and O–C=O (290.7 eV) groups (Fig. 4b). The Sn 3d spectrum (Fig. 4c) shows two symmetric peaks at around 487.5 eV and 495.8 eV, which are characteristic of Sn 3d$_{5/2}$ and Sn 3d$_{3/2}$, respectively. The presence of Sn in the (+4) state confirms the formation of only the SnO_2 phase in the solar reduced SnO_2/gC composite. Fig. 4d shows the Sn 3d peaks for SnO_2/MWNT, with similar features to SnO_2/gC, thus confirming the formation of the tin(IV) oxide phase. 40–60 nm average diameter multiwalled carbon nanotubes with lengths of a few μm (Fig. 5a) were synthesized using the CCVD technique. The TEM image in Fig. 5b shows the inner hollowness of the synthesized MWNT. The average number of layers of nanotubes

was found to be ~25–30. Tin oxide nanoparticles decorated over the smooth MWNT surface make the surface rough (Fig. 5c), which correlates with the higher I_D/I_G value. Distinct particles decorated over the smooth MWNT surface can be seen in the TEM image of SnO_2/MWNT (Fig. 5d). The TEM image of the gC structure shows 10–20 nm uniform graphene wrapping over a 50–70 nm diameter nanotube structure (Fig. 6a). The SnO_2 nanoparticles that are uniformly dispersed over this composite are visible in the TEM image of SnO_2/gC (Fig. 6b). The HRTEM image (Fig. 6c) of the same composite shows spherical nanoparticles with average sizes of 2.9 nm. The EDAX spectrum shown in Fig. 6d shows the desired presence of Sn, oxygen and carbon in the synthesized structure. The homogeneous distribution of a Sn and O lattice over the carbon surface has also been confirmed by the elemental mapping of SnO_2/gC (Fig. S1†).

Electrochemical characterization was carried out on the fabricated CR 2032 cells, after confirmation of the phase formation of the desired material, and the results are presented in Fig. 7 and 8. Fig. 7a shows the Li$^+$ insertion and extraction process in the form of cyclic voltammograms (CV) for SnO_2/gC over the range of 3–0.01 V (vs. Li/Li$^+$) at a scan rate of 0.5 mV s^{-1}. The material shows two main sets of anodic and cathodic peaks at similar potential positions to those of tin oxide. The slightly shifted oxidation and reduction peaks might be due to the separate polarization as a result of hybridization of the carbon support and tin oxide nanoparticles. The CV for the first cycle is clearly distinct compared to those of the other cycles for the peak at around 0.7–1.3 V. This represents both the well-known solid electrolyte interphase (SEI) formation[31] and the reduction of tin oxide to tin, resulting in the formation of Li_2O[32] (eqn (1)). The lower intensity of this peak in the consequent cycles confirms the low reversibility of SEI layer formation. The broad peak from 0.5 V to 0.01 V represents the alloying of tin (eqn (2)).
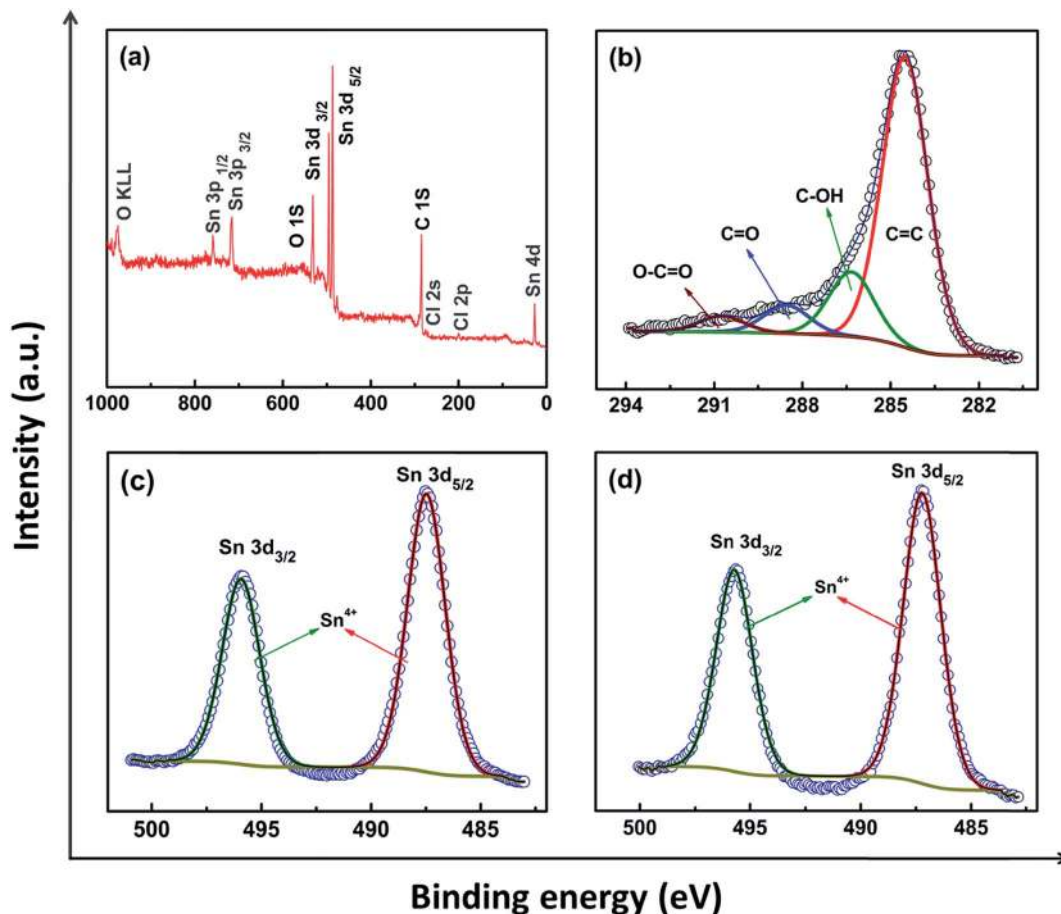
Fig. 4 XPS study: (a) survey spectrum, deconvoluted spectra for (b) C 1s and (c) Sn 3d for SnO_2/gC respectively; (d) deconvoluted spectrum of Sn 3d for $SnO_2/MWNT$.
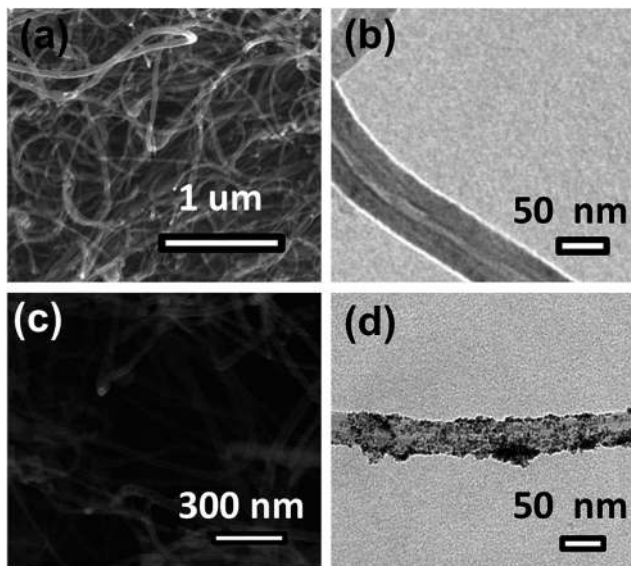

Fig. 5 SEM and TEM images (a and b, respectively) of MWNT, and (c and d, respectively) $SnO_2/MWNT$.

The cathodic peak at 0.25 V represents the interaction of Li^+ with the carbon layers (eqn (3)). The peaks at around 0.7 V and 1.4 V represent the de-alloying and oxidation into SnO_2, respectively (backward reactions of eqn (1) and (2)). Though the conventional method of theoretical capacity calculation for SnO_2 considers the backward reaction of eqn (1) to be completely irreversible, the present voltammogram shows a prominent and stable peak at 1.42 V, even after 10 cycles, suggesting the enhanced capacity of the investigated material as a Li ion battery anode. The uniform dispersion of SnO_2 nanoparticles over the protruding graphene wrapped multi-walled carbon nanotubes, as seen in the TEM image of Fig. 6b and c, can also be confirmed from the consistency of the anodic peak at 0.7 V (backward reaction of eqn (2)). This peak also proves the involvement of Li interaction in the composite from the very first cycle without any activation.[33] The repeatability of the voltammogram also suggests high cyclability by possibly confining the formed Li_xSn and Li_2O into the accommodating structure of SnO_2/gC.
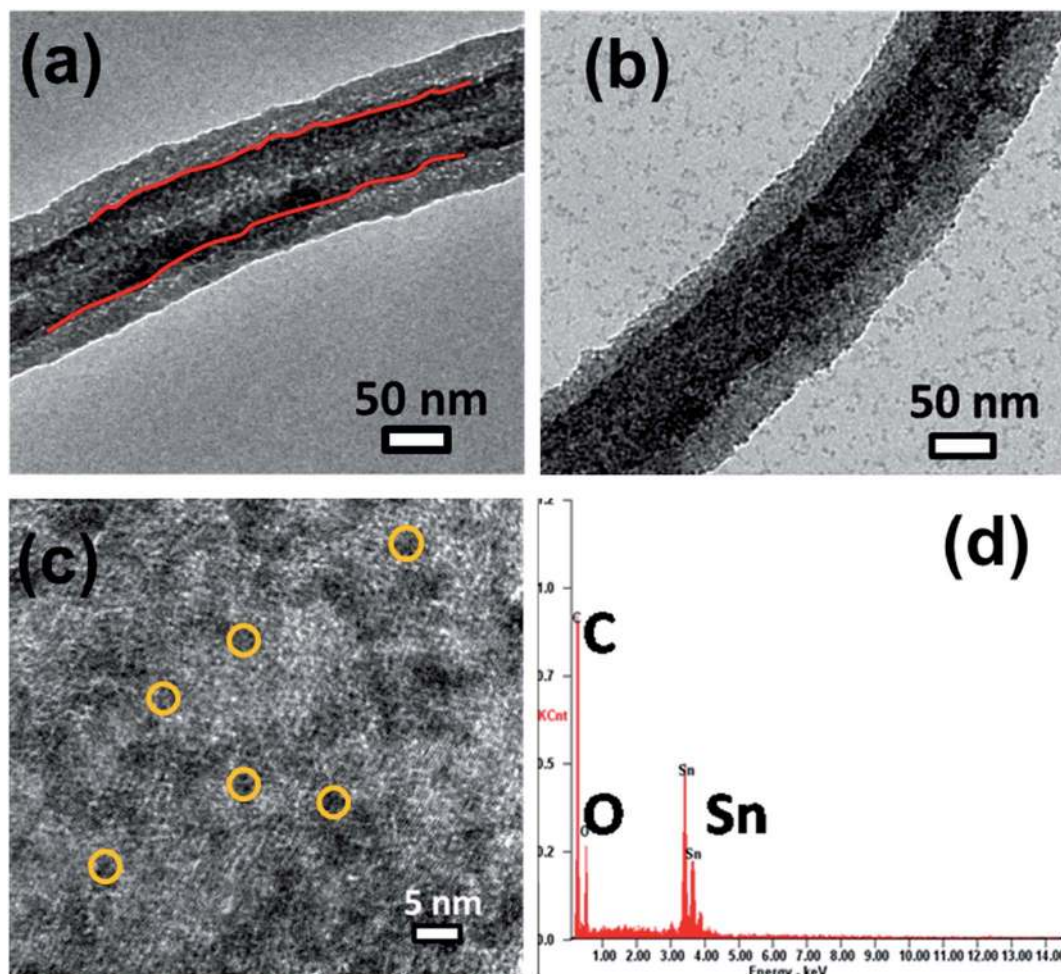
$$SnO_2 + 4Li^+ + 4e^- \leftrightarrow Sn + 2Li_2O \tag{1}$$

$$Sn + xLi^+ + xe^- \leftrightarrow Li_xSn \ (0 \leq x \leq 4.4) \tag{2}$$
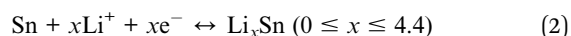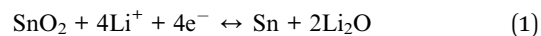
Fig. 6 (a) SEM image of the employed gC; (b) TEM and (c) HRTEM images and (d) the EDAX spectrum of SnO_2/gC.
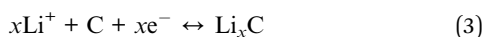
$$xLi^+ + C + xe^- \leftrightarrow Li_xC \tag{3}$$

Fig. 7b shows galvanostatic charge discharge studies of SnO_2/gC as a LIB anode material at different current densities. The first discharging capacity for SnO_2/gC at a current density of 50 mA g^{-1} was 1675 mA h g^{-1}, with 920 mA h g^{-1} as the charging capacity and a 55% initial coulombic efficiency. $SnO_2/MWNT$ shows a 907 mA h g^{-1} discharge capacity in the first cycle with a 53% coulombic efficiency at the same current density (Fig. 8a). The discharge capacity value goes down to 1025 mA h g^{-1} for SnO_2/gC and 533 mA h g^{-1} for $SnO_2/MWNT$ in the next cycle. This irreversible loss is attributed to the electrolyte decomposition, and SEI layer and Li_2O formation[32] (Fig. 7c). The coulombic efficiency increases to 87% and 86% in the next cycle for SnO_2/gC and $SnO_2/MWNT$, respectively. The rate capability test for SnO_2/gC shown in Fig. 7c shows the capacity restoration when the current density is varied, thus confirming the reversibility of the anode. At higher current densities of 100 mA g^{-1}, 250 mA g^{-1} and 500 mA g^{-1}, the achieved discharge/charge capacities were 543/497 mA h g^{-1}, 325/324 mA h g^{-1} and 163/161 mA h g^{-1}, respectively for SnO_2/gC

(Fig. 7c). A constant discharge capacity of 333 mA h g^{-1} with a 99% coulombic efficiency was achieved after 65 cycles at a current density of 250 mA g^{-1}, emphasizing the superior rate capability. The cyclic stability test at a current density of 50 mA g^{-1} for SnO_2/gC in comparison to $SnO_2/MWNT$ is shown in Fig. 8b. For $SnO_2/MWNT$ as an anode material, the discharge capacity reduces to 231 mA h g^{-1} after 50 cycles with a 57% declining capacity, thus suggesting poor cyclability (Fig. 8b(i)). SnO_2/gC shows a 592 mA h g^{-1} capacity at the end of 100 cycles, with only a 16% capacity fading with respect to the second cycle (Fig. 8b(ii)). The electrochemical specific capacity of SnO_2/gC is higher than those of the reported microwave reduced SnO_2/G-CNT composite[18] and flexible SnO_2/G-CNT paper.[15] Other SnO_2 decorated 1D–2D composite materials (Table 2) showed higher performances compared to the present tin oxide decorated graphene wrapped carbon nanotubes. The lower capacity of SnO_2/gC can be countered by consideration of the higher loading of metal oxide on the 1D–2D hybrid support and the complicated synthesis processes of the composite materials. The employed SnO_2/gC exhibits comparable performance to the reported 649 mA h g^{-1} for a 2D SnO_2/G anode with higher loading of tin oxide.[34] Evidently, the 1D SnO_2/gC structure
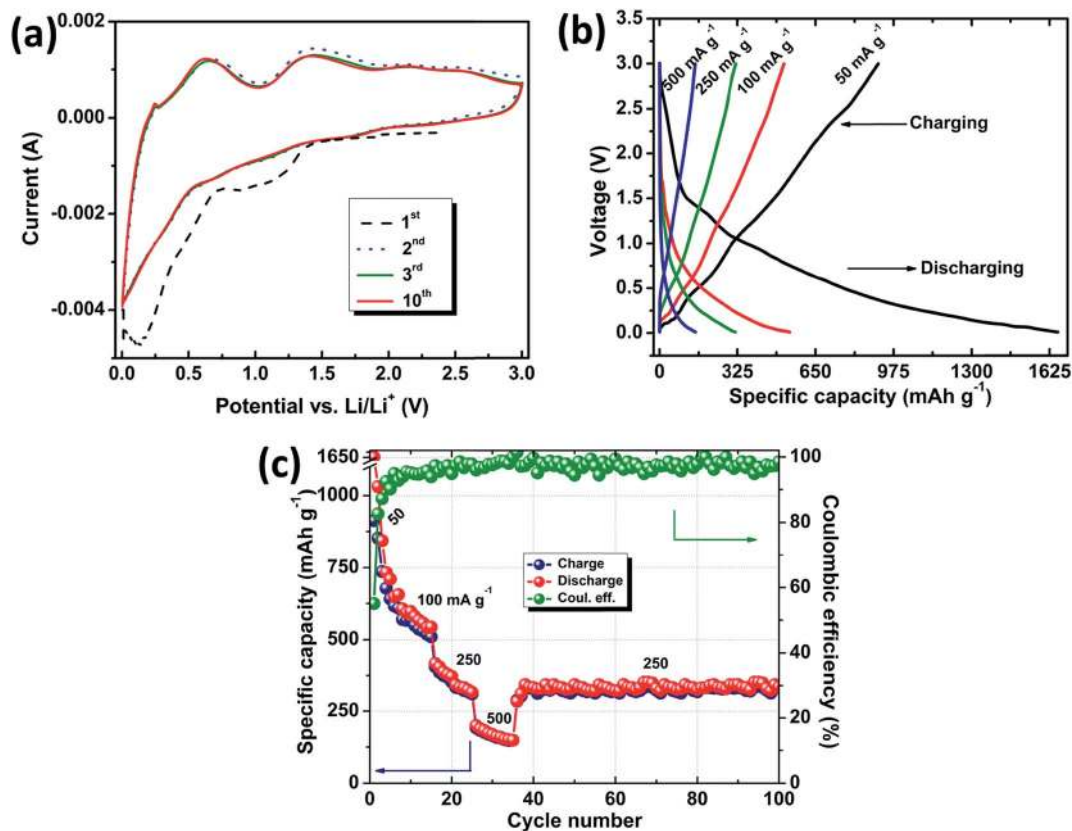
Fig. 7 Electrochemical studies of SnO_2/gC: (a) cyclic voltammograms at a scan rate of 0.5 mV s^{-1}, (b) charge–discharge profiles and (c) rate capability tests at various current densities.

shows higher capacity and stability compared to the investigated wrinkle-free 1D SnO_2/MWNT. The high conductivity of the inner core of gC leads to a high rate of electron transfer. Wrinkly defects in the gC surface enhance the anchoring sites for SnO_2 together with the higher Li storage and interaction probability. The synergistic effect of these two factors suggests that SnO_2/gC is a high rate capable and stable anode material for Li ion batteries with a higher specific discharge capacity of 592 mA h g^{-1}.

Electrochemical impedance spectroscopy (EIS) measurements for SnO_2/gC in comparison with SnO_2/MWNT are represented in Fig. 8c as Nyquist plots for further investigation. The measurements were carried out by employing a sine wave with an amplitude of 5 mV over a frequency range of 100 kHz to 0.01 Hz. The spectra were recorded after 100 cycles of charge–discharge at a 500 mA g^{-1} current density, to obtain detailed information about the SEI layer, resistances and diffusion of Li within the cell. An equivalent circuit was modeled to analyze the spectra (Fig. 8d). Z-view software was used to simulate the plot using the equivalent circuit. The simulation shows a depressed semicircle with two partially overlapping contributions and a sloping line. The intercept at the real axis (Z') at high frequencies is attributed to the overall ohmic resistance, including contributions from the separator, electrolyte and all electrical connections (R_e). The high frequency semicircle arises due to Li$^+$ ion migration through the SEI layer and is

represented by R_{SEI} and charge phase elements. The low frequency semicircle takes into account the charge transfer resistance (R_{ct}) and the corresponding constant phase element of the electrode/electrolyte. The straight line represents the Warburg impedance (W) of the diffusion of Li ions into the electrode. The perfect fitting of the simulated curve with the experimental spectra is in agreement with the perfectly selected equivalent circuit and parameters. The lower R_e values of SnO_2/MWNT compared to those of SnO_2/gC can be attributed to the higher conductivity of the crystalline and smoother surface backbone of MWNT. The lower R_{SEI} value for SnO_2/gC compared to that of SnO_2/MWNT points to the probability of restricting the SEI layer thickness and the improved ion pathways for the unique structure of the graphene wrapped carbon nanotubes support (Table 3). Charge transfer resistance, R_{ct}, is also lower for tin oxide nanoparticles supported graphene wrapped carbon nanotubes over SnO_2/MWNT resulting improved exchange current density ($i_0 = RT/nFR_{ct}$). The lower total cell resistance of SnO_2/gC results in enhanced reaction kinetics, thus ensuring a higher rate capability and improved cyclability as an anode material compared to only MWNT, gC[19] and SnO_2/MWNT for Li ion batteries.

Solar reduction results in optimized 3 nm particles of SnO_2 over the graphene wrapped carbon nanotubes. The probability of agglomeration is also less for the gC support due to wrinkled surface defects in comparison with MWNT. This
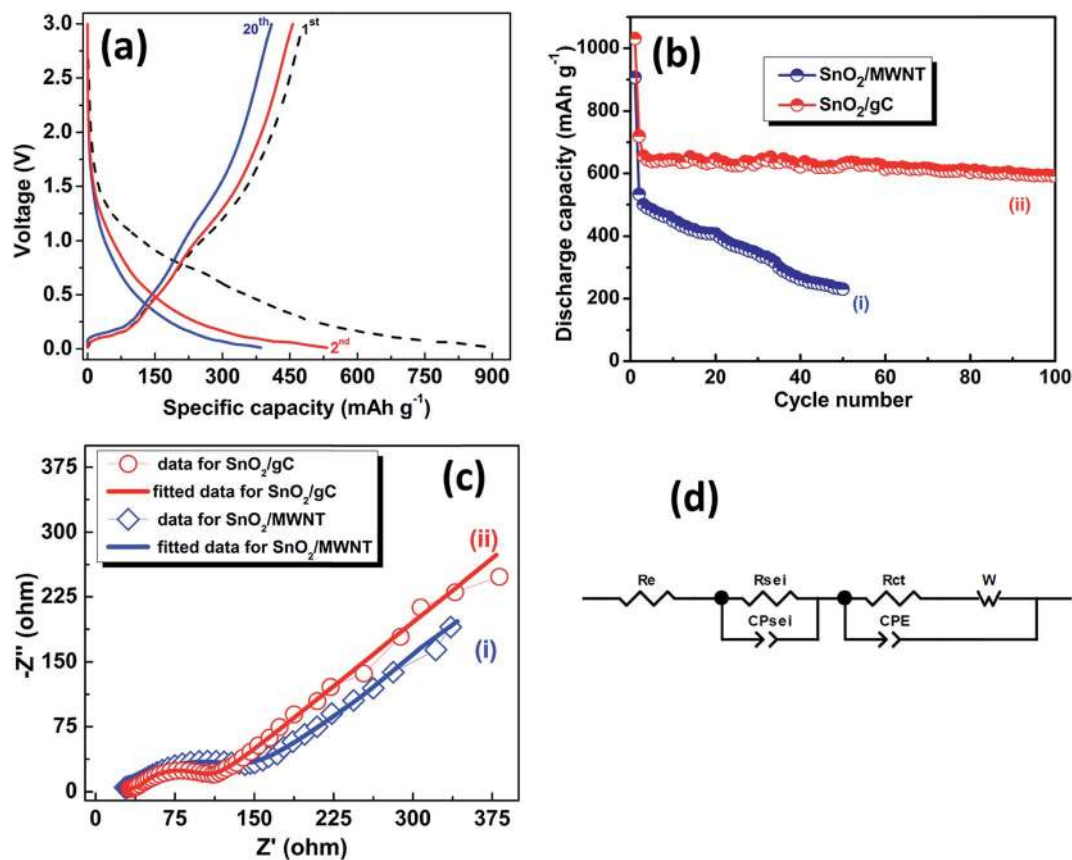
Fig. 8 (a) Charge–discharge profiles at a 50 mA g^{-1} current density for SnO$_2$/MWNT, (b) stability tests and (c) electrochemical impedance study for (i) SnO$_2$/MWNT, and (ii) SnO$_2$/gC; (d) equivalent circuit model fitted to the Nyquist plots.

interconnected-porous structure of gC also provides breathing space for the volume expansion of the nanoparticles during lithiation/delithiation (Fig. 1). By compensating for the semi-conducting nature of SnO$_2$ and accommodating the strain released due to volume change in the lithiation/delithiation process, the interconnected nano-3D conducting composite structure, SnO$_2$/gC, proved to be a prospective anode material for LIBs with higher stability. Carbon coating over tin oxide nanoparticles to balance the semiconducting nature and heteroatom doping in the gC support for enhanced electrical

Table 3 Impedance parameters for the investigated anode materials, calculated from the equivalent model

Material	R_e	R_{SEI}	R_{ct}
SnO$_2$/MWNT	17.24	36.55	86.92
SnO$_2$/gC	29.31	11.91	63.9

conductivity can still be employed, and an improved, higher performance for SnO$_2$/carbon composite structures as an anode for Li ion batteries is anticipated.

Table 2 Performance comparisons of SnO$_2$/gC as an anode material for Li ion batteries^a

Anode material employed	Dimension of employed support nanostructure	Current density (mA g^{-1})	Specific capacity (mA h g^{-1})	
			Initial discharge/charge	Reversible [cycle no.]
80% SnO$_2$–G[34]	2D	50	2140/1080	649 [30]
60% SnO$_2$/G-CNT[18]	1D–2D	100	∼1050/*	502 [50]
83.5% SnO$_2$/G-CNT[16]	3D aerogel	200	∼1806/1200	842 [40]
45% SnO$_2$-PG/CNW[17]	1D–2D	200	∼950/*	943 [50]
63% SnO$_2$/G-CNT[15]	1D–2D	250	∼1600/820	635 [80]
Flexible SnO$_2$/G-CNT paper[15]	1D–2D	100	∼990/400	387 [50]
SnO$_2$/MWNT	**1D**	**50**	**907/480**	**231 [50]**
SnO$_2$/gC (present work)	**1D**	**50**	**1675/920**	**592 [100]**

^{a} *Denotes data not available.

Conclusions

Tin oxide decorated graphene wrapped carbon nanotube structure was synthesized using a one pot, simple and green solar reduction technique. Graphene wrapping in the form of protrusions acts as an easy and strong anchoring site for nanoparticle decoration, thus preventing the agglomeration of nanoparticles over cycles. The conducting monohybrid structure of the gC support improves the electron transfer, thus compensating for the semiconducting tin oxide. Protruding surface tubes, as individuals as well as bunches, provide better Li^+ pathways. The nano-architecture of the SnO_2/gC composite with improved reaction kinetics thus shows an improved, stable capacity of 592 mA h g^{-1} at 50 mA g^{-1} after 100 cycles by accommodating the volume change in its porous structure.

Acknowledgements

References

1 J. B. Goodenough and K. S. Park, *J. Am. Chem. Soc.*, 2013, **135**, 1167–1176.

2 C. Wang, A. J. Appleby and F. E. Little, *J. Electroanal. Chem.*, 2001, **497**, 33–46.

3 Q. Zhou, L. Yang, G. Wang and Y. Yang, *Biosens. Bioelectron.*, 2013, **49**, 25–31.

4 S. Byun and B. Shin, *J. Mater. Chem. A*, 2016, **4**, 16175–16183.

5 H. Wang and A. L. Rogach, *Chem. Mater.*, 2014, **26**, 123–133.

6 L. Liu, F. Xie, J. Lyu, T. Zhao, T. Li and B. G. Choi, *J. Power Sources*, 2016, **321**, 11–35.

7 K. Kisu, M. Iijima, E. Iwama, M. Saito, Y. Orikasa, W. Naoi and K. Naoi, *J. Mater. Chem. A*, 2014, **2**, 13058–13068.

8 C. Kim, M. Noh, M. Choi, J. Cho and B. Park, *Chem. Mater.*, 2005, **17**, 3297–3301.

9 X. W. Lou, Y. Wang, C. Yuan, J. Y. Lee and L. A. Archer, *Adv. Mater.*, 2006, **18**, 2325–2329.

10 X. L. Wang, M. Feygenson, M. C. Aronson and W. Q. Han, *J. Phys. Chem. C*, 2010, **114**, 14697–14703.

11 Z. Wen, Q. Wang, Q. Zhang and J. Li, *Adv. Funct. Mater.*, 2007, **17**, 2772–2778.

12 L. S. Zhang, L. Y. Jiang, H. J. Yan, W. D. Wang, W. Wang, W.-G. Song, Y.-G. Guo and L. J. Wan, *J. Mater. Chem.*, 2010, **20**, 5462–5467.

13 S. Ding, D. Luan, F. Y. C. Boey, J. S. Chen and X. W. Lou, *Chem. Commun.*, 2011, **47**, 7155–7157.

14 M. Sahoo and S. Ramaprabhu, *Graphene*, 2014, **2**, 88–94.

15 B. Zhang, Q. B. Zheng, Z. D. Huang, S. W. Oh and J. K. Kim, *Carbon*, 2011, **49**, 4524–4534.

16 Z. Zhang, L. Wang, J. Xiao, F. Xiao and S. Wang, *ACS Appl. Mater. Interfaces*, 2015, **7**, 17963–17968.

17 J. Tang, J. Yang, X. Zhou, H. Yao and L. Zhou, *J. Mater. Chem. A*, 2015, **3**, 23844–23851.

18 T. Chen, L. Pan, X. Liu, K. Yu and Z. Sun, *RSC Adv.*, 2012, **2**, 11719–11724.

19 M. Sahoo and S. Ramaprabhu, *Electrochim. Acta*, 2015, **186**, 142–150.

20 S. Venkateswarlu, D. Lee and M. Yoon, *ACS Appl. Mater. Interfaces*, 2016, **8**, 23876–23885.

21 K. R. Reddy, B. C. Sin, C. H. Yoo, W. Park, K. S. Ryu, J.-S. Lee, D. Sohn and Y. Lee, *Scr. Mater.*, 2008, **58**, 1010–1013.

22 K. R. Reddy, M. Hassan and V. G. Gomes, *Appl. Catal., A*, 2015, **489**, 1–16.

23 K. R. Reddy, B. C. Sin, C. H. Yoo, D. Sohn and Y. Lee, *J. Colloid Interface Sci.*, 2009, **340**, 160–165.

24 S. S. Jyothirmayee Aravind, V. Eswaraiah and S. Ramaprabhu, *J. Mater. Chem.*, 2011, **21**, 15179–15182.

25 P. Nayak, P. N. Santhosh and S. Ramaprabhu, *J. Phys. Chem. C*, 2014, **118**, 5172–5179.

26 M. Baro, P. Nayak, T. T. Baby and S. Ramaprabhu, *J. Mater. Chem. A*, 2013, **1**, 482–486.

27 A. L. M. Reddy, M. M. Shaijumon and S. Ramaprabhu, *Nanotechnology*, 2006, **17**, 5299.

28 A. L. Patterson, *Physical Review*, 1939, **56**, 978–982.

29 A. Diéguez, A. Romano-Rodríguez, A. Vilà and J. R. Morante, *J. Appl. Phys.*, 2001, **90**, 1550–1557.

30 J. Xu, Y. Li, H. Huang, Y. Zhu, Z. Wang, Z. Xie, X. Wang, D. Chen and G. Shen, *J. Mater. Chem.*, 2011, **21**, 19086–19092.

31 Z. Wang, G. Chen and D. Xia, *J. Power Sources*, 2008, **184**, 432–436.

32 H. J. Ahn, H. C. Choi, K. W. Park, S. B. Kim and Y. E. Sung, *J. Phys. Chem. B*, 2004, **108**, 9815–9820.

33 G. Du, C. Zhong, P. Zhang, Z. Guo, Z. Chen and H. Liu, *Electrochim. Acta*, 2010, **55**, 2582–2586.

34 X. Zhu, Y. Zhu, S. Murali, M. D. Stoller and R. S. Ruoff, *J. Power Sources*, 2011, **196**, 6473–6477.